Reliability-Driven Assessment of GaN HEMTs and Si IGBTs in 3L-ANPC PV Inverters

Emre Gurpinar, *Student Member, IEEE*, Yongheng Yang, *Member, IEEE*,
Francesco Iannuzzo, *Senior Member, IEEE*, Alberto Castellazzi,
and Frede Blaabjerg, *Fellow, IEEE*

***Abstract*— In this paper, thermal loading of the state-of-the-art gallium nitride (GaN) High-electron-mobility transistors (HEMTs) and traditional Si Insulated-gate bipolar transistors (IGBTs) in three-level active neutral-point-clamped photovoltaic inverters is presented considering real-field long-term mission profiles (i.e., ambient temperature and solar irradiance). A comparison of Si IGBT against GaN HEMT with three different possibilities: 1) with thermal interface material (TIM) at 10 kHz; 2) without TIM at 10 kHz; and 3) with TIM at 300 kHz has been performed. The assessment results indicate lower thermal stress with GaN HEMT devices at 10 kHz in comparison with Si IGBT. At high switching frequencies, the results show that the significant system level cost savings can be achieved without compromise of operating efficiency with GaN HEMTs. Both simulations and experimental tests are provided to demonstrate the thermal loading analysis approach. More important, the proposed analysis and comparison approach can be used for lifetime and reliability analysis of wide bandgap devices.**

***Index Terms*— Gallium nitride (GaN), photovoltaic (PV) systems, reliability, thermal loading analysis, three-level active neutral-point-clamped (3L-ANPC) converter, wide bandgap (WBG) power devices.**

I. Introduction

RENEWABLE power generation is one of the main focus areas of highly efficient power electronic systems due to the increasing demand for clean power resources. Photovoltaic (PV) energy is a key renewable energy resource along with hydro and wind, and as of 2013, the global installed PV capacity has been over 138 GW with a potential of 160-TWh energy generation every year. In addition to the current-installed capacity, the worst case scenario for annual PV installation until 2018 is expected to be around 35 GW [1]. Even with the worst case scenario, there is a strong demand for energy generation with PV systems, where power electronic converters are the vital components for the realization of this demand. Basically, the power electronic converters provide two main tasks for PV systems: 1) maximization of energy utilization by means of maximum power point tracking (MPPT) control and 2) integration with an ac grid by converting the generated electricity from dc to ac (i.e., using dc–ac inverters) in a grid-friendly manner. That is to say, a certain amount of demands to PV systems should be taken into account in the planning, design, and operation phases. For instance, different converter topologies and system structures based on single- and double-staged conversion systems are published and reviewed in the literature [2]–[4], whereas the aforementioned power electronics converters are widely utilized.

For the maximization of energy generation and the minimization of system payback time, the efficiency of power electronic converters in PV applications is always one of the key parameters along with reliability and lifetime in those applications. Therefore, the efficiency improvement of power electronic systems has been an important aspect of research in renewable energy. Transformerless inverter topologies have been proposed that introduce additional power switches for maintaining high efficiency while minimizing the leakage ground current without the presence of the galvanic isolation between PV panels and the grid [5], [6]. Along with new transformerless topologies, emerging wide bandgap (WBG) devices, such as SiC Schottky diodes, SiC junction gate field-effect transistors (JFETs), SiC Metaloxide semiconductor field-effect transistors (MOSFETs), and gallium nitride (GaN) High-electron-mobility transistors (HEMTs), have been introduced to PV converters due to superior properties of WBG materials [7]. The application of WBG devices in dc/dc converters and dc/ac inverters for PV systems has been widely discussed in the literature. Various converters with different application conditions show the potential of achieving very high efficiencies with WBG devices under a wide operating range.

For example, the performance of SiC JFET devices for PV applications has been discussed in detail in [8]–[10]. A number of experimental test results show a peak efficiency of 98.8%, and in [8], the highly efficient and reliable inverter concept converter with SiC devices has achieved a 99% peak efficiency. As demonstrated in [9], the overall losses in a PV inverter can be halved by just replacing the conventional Si Insulated-gate bipolar transistors (IGBTs) with the SiC JFETs, and thus, the efficiency can be improved. Although SiC JFETs had promising results, the gate drive complexity and normally-on characteristic of the devices were the main obstacles for

Manuscript received January 10, 2016; revised April 28, 2016; accepted May 4, 2016. Recommended for publication by Associate Editor Jin Wang (GE).

E. Gurpinar and A. Castellazzi are with the Power Electronics, Machines and Control Research Group, University of Nottingham, Nottingham NG7 2RD, U.K. (e-mail: emre.gurpinar@nottingham.ac.uk; alberto.castellazzi@nottingham.ac.uk).

Y. Yang, F. Iannuzzo, and F. Blaabjerg are with the Department of Energy Technology, Aalborg University, Aalborg 9220, Denmark (e-mail: yoy@et.aau.dk; fia@et.aau.dk; fbl@et.aau.dk).

Color versions of one or more of the figures in this paper are available online at http://ieeexplore.ieee.org.

Digital Object Identifier 10.1109/JESTPE.2016.2566259

applications in commercial products [11]. Alternatively, SiC MOSFETs have been introduced at 600 and 1200 V blocking class range for renewable applications from different manufacturers, and the performances of these devices in various topologies are discussed in [12]–[14]. Similar to the results with SiC JFETs, replacing Si IGBTs with SiC MOSFETs can bring up to 1% efficiency gain for the same switching frequency. In [13], the performance of SiC MOSFETs and Si IGBTs at 600 V class has been presented, where it shows that the SiC MOSFETs under different ambient temperatures can operate without malfunctions. In addition, all SiC-based three-level T-type inverters can achieve the peak efficiency of 98.3% at 16-kHz switching frequency.

Recent findings show that the WBG power devices suitable for grid-connected applications are normally-off GaN HEMTs at a blocking class of 600 V. Such GaN normally-off HEMTs have been introduced by Panasonic at 600 V and GaN Systems at 650 V. There are several practical applications with those WBG devices. For instance, in [15], GaN HEMTs are implemented in a dc/dc converter for the MPPT control in PV applications, and the converter operated with a peak efficiency of 98.59% at 48-kHz switching frequency. Furthermore, the same devices have been used in other applications, such as resonant LLC dc/dc converters, three-phase inverters, and synchronous buck converters. Those cases have shown the high switching and conduction performance of the GaN HEMT devices in different operating conditions [16]–[20]. Specifically, in [17], GaN devices are demonstrated on a three-phase inverter with 99.3% efficiency at 900-W output power and 16-kHz switching frequency. Finally, GaN HEMTs are demonstrated along with 1200 V SiC MOSFETs in single-phase PV applications in [19] and [20], where the converter has achieved 99.2% peak efficiency at 1.4-kW output power and 16-kHz switching frequency. The presented converter proves the stable operation of WBG devices under wide load, switching frequency, and ambient temperature conditions. Furthermore, normally-on GaN HEMTs at 600 V voltage class with and without cascode structures are discussed in [21] and [22] for hard-switching topologies. Performance improvement in a synchronous buck topology is presented in [21], and it is shown that smaller reverse recovery charge and output capacitance of GaN HEMTs lead to reduction in turn-on losses and up to 2% efficiency improvement in comparison with Si MOSFET. The current collapse phenomena for 600 V normally on GaN HEMT is presented in [22]. Although the device is statically rated at 600 V, the experimental results are presented up to 50–60 V due to the increase in on-state voltage drop during dynamic testing. Nevertheless, the above literature survey shows that the WBG-based power converters can deliver very high efficiency at switching frequencies that is not possible with the conventional Si-based power devices.

In addition to high efficiency, high reliability is required for PV inverters in order to extend the lifetime of the system and therefore energy generation [23], and as a consequence to reduce the cost of energy. Commercial PV inverters are generally offered with a 25 year performance warranty, and also considered as the most vulnerable components in a PV system [24]. It is known from field data that a majority of

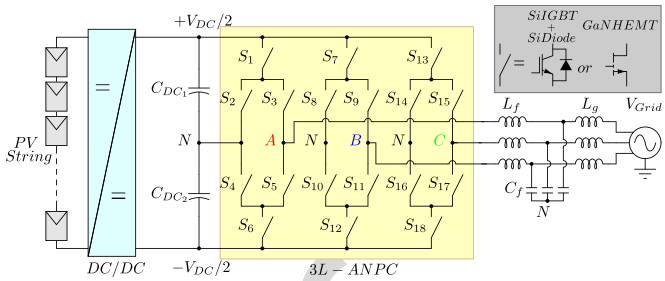

Fig. 1. Grid-connected three-phase double-stage 3L-ANPC inverter with an LCL filter in PV applications.

the failure mechanisms for PV inverters are related to mean temperature variations and temperature swings [25]; therefore, long-term mission profile plays a key role in reliability and assessment of thermal performance of the inverter [26], [27]. During the design process, real-field operating conditions (e.g., ambient temperature and solar irradiance) have to be considered for reliability-oriented approaches, as different conditions may unevenly stress the components within the system. Emerging SiC and GaN power devices have different electrical and thermal properties from Si devices due to inherent differences in material, chip size, and packaging properties [28]. Therefore, it is essential to evaluate the long-term performance of the system for better understanding the benefits as well as the drawbacks of using WBG devices in PV systems. In such a way, the applications of WBG devices can further be paved away.

In this paper, a reliability-oriented comparison of the conventional Si IGBTs with the state-of-the-art GaN HEMTs for three-level active neutral-point-clamped (3L-ANPC) PV systems is thus presented. In Section II, converter topology, modulation strategy, and power device properties are presented, followed by a mission-profile oriented analysis in terms of thermal loading and reliability estimation of the considered power electronic converters. Simulation results of the converter based on GaN and Si devices are presented in Section III regarding efficiency, annual energy generation, loss distribution, and thermal loading. Finally, the experimental results of the GaN-based prototype (i.e., 3L-ANPC inverter) at different load conditions are presented before the conclusion.

II. 3L-ANPC Inverter and PV System

A. ANPC Topology and Modulation Scheme

ANPC inverter is a member of half-bridge NPC inverter family and it was introduced in [29] as an alternative to NPC inverter [30] for improved loss balancing and better utilization of semiconductor chip areas in the inverter. Replacing diodes in NPC inverters with active switches provides additional zero states, and at the same time, different modulation strategies can be applied with a flexible utilization of the redundant switching states. The topology has been discussed thoroughly for industrial drive applications in the literature [31]–[33]. The schematic of the studied converter for a double-stage three-phase grid-connected PV system is shown in Fig. 1. As it can be observed, each leg of the 3L-ANPC inverter

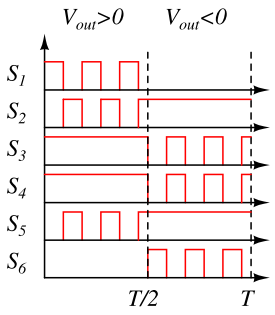

Fig. 2. Switching sequences for leg-A of the 3L-ANPC inverter [12].

is formed by six active switches (S_1–S_{18} of three legs) in order to achieve a three-level phase output voltage with respect to the neutral point N, and the power devices (S_1–S_{18}) are rated at half of the dc-link voltage $V_{\rm dc}$. Consequently, it is possible to use GaN HEMT devices at 600 V class for three-phase grid-connected applications, where the dc-link voltage is within a range of 650–1000 V. In this configuration, a dc–dc converter between the PV strings and the 3L-ANPC inverter is adopted in order to flexibly maximize the energy production (i.e., MPPT control) as well as to extend the operating hours of the PV systems (e.g., in the case of weak solar irradiance). The power delivered by the dc/dc converter is then fed to the 3L-ANPC inverter, while the dc-link voltage is usually maintained as constant by controlling the inverter. Normally, for the PV system, it should inject high-quality grid currents at unity power factor operation, and thus, the modulation schemes applied to the 3L-ANPC inverter should be specially designed.

Different modulation strategies can be implemented for the 3L-ANPC inverter in order to achieve a balanced switching loss distribution or doubling of the effective switching frequency at the output [34]. Solutions proposed in [31]–[33] and [35] are limited to the use of Si devices and were optimized for IGBTs as well as for MOSFETs. A modulation strategy based on the reverse conduction capability of SiC MOSFETs has been introduced in [12] for a single-phase leg, as further shown in Fig. 2. It can be seen from the driving signals that there are four operating states: 1) positive voltage; 2) zero-state positive current; 3) zero-state negative current; and 4) negative voltage. Specifically, taking leg-A shown in Fig. 1 as an example, the positive voltage is applied to the output of the phase leg by turning-on S_1 and S_3, and the output current flows through the two devices in series. During the positive active-state, S_4 ensures an equal dc-link voltage sharing between S_5 and S_6 without conducting any current. The transition from positive active state to zero state is accomplished by switching S_1 off, and then simultaneously switching S_2 and S_5 on, and thus, the current is divided in two parallel paths: S_2–S_3 and S_4–S_5. The same commutation scheme is used for complementary switches during the negative active state and the zero state. This modulation method ensures low conduction losses at zero states, and the outer switches (S_1 and S_6) are exposed to switching losses at unity power factor. In a Si-based converter, IGBTs with antiparallel diodes can be employed, while in GaN-based converter, only HEMTs will be sufficient because of the reverse conduction capability of HEMT devices. Therefore, although the number of active devices in Si and GaN will be the same, the number of total switches will be half in GaN-based inverter due to the absence of antiparallel diodes, leading to reduced converter volume as well as heatsink size.

TABLE I
CONVERTER AND SYSTEM PARAMETERS

Parameter	Value
Input DC Link Voltage (V_{DC})	800 V
Input Power (P_{in}) @ 25 ^{o}C, 1000 W/m^2	6 kW
Switching Frequency (f_{sw})	10 kHz - 300 kHz
DC Link Capacitor ($C_{DC_1} - C_{DC_2}$)	1500 μF
Output Filter Inductor (L_f)	3.6 mH
Output Filter Capacitor (C_f)	2.35 μF
Output Filter Capacitor (L_g)	4 mH
Grid Phase-to-Phase Voltage (V_{ph-ph})	400 Vrms
PV Module	BP 365
PV String Configuration	46 module each - 2 strings
DC/DC (MPPT) Efficiency (η_{MPPT})	99 %

B. System and 3L-ANPC Parameters

The PV system and converter parameters considered in this paper are presented in Table I. As the dc/dc converter between the PV strings and the 3L-ANPC inverter that is shown in Fig. 1 is responsible from the MPPT control, it is assumed that the conversion efficiency of 99% can be achieved by the MPPT control of the converter in the following. Recent advances in SiC MOSFETs show that the efficiency higher than 99% is feasible for dc/dc converters in PV applications [36]. Two parallel-connected PV strings, formed by 46 PV modules, are considered to deliver 6-kW power at the standard test conditions (i.e., 25 °C ambient temperature and 1000-W/m^2 solar irradiance). The input power $P_{\rm in}$ can go up to 11 kW at −25 °C and 1500 W/m^2 theoretically, and therefore, the total rating of the converter is selected as 15 kW in order to operate at a wide range of ambient temperature and solar irradiance. The inverter is operated at 10 kHz switching frequency for Si IGBTs, while at 10 and 300 kHz for GaN HEMT devices for the evaluation of the performance of GaN HEMT-based inverter at low and high switching frequencies in comparison with the Si IGBT-based inverter. The selection of 300 kHz for high-frequency application of the GaN HEMTs is determined by the operation point of the converter, where the junction temperature of the most stressed devices is close to their limits, and the efficiency is still higher than the Si IGBT-based converter. In addition, it is shown in [37] that by moving from 10 to 300 kHz, 70% reduction in Electro Magnetic Compatibility filter volume can be achieved for GaN HEMTs.

C. 650 V GaN HEMT and 600 V Si IGBT

As previously discussed, the GaN HEMT devices have superior switching properties in comparison with Si IGBTs

TABLE II
GaN HEMT AND Si IGBT PROPERTIES

	GaN Systems GaN E-HEMT GS66508T	Infineon Si IGBT IKP20N60H3
Drain-Source Voltage (V_{DS})	650 V	600 V
Continuous Drain Current (I_{DS})	23 A @ 100 °C	20 A @ 100 °C
Drain-Source On-State Resistance ($R_{DS_{ON}}$)	55 mΩ @ 25 °C 129 mΩ @ 100 °C	N/A
Collector-Emitter Saturation Voltage ($V_{CE_{Sat}}$)	N/A	1.95 V @ 25 °C 2.5 V @ 100 °C
Input Capacitance (C_{iss})	200 pF	1100 pF
Output Capacitance (C_{oss})	67 pF	70 pF
Reverse Transfer (C_{rss})	2 pF	32 pF
Gate Charge (Q_g)	6.5 nC	120 nC
Min. Gate Threshold Voltage (V_{th})	1.6 V	4.1 V
Maximum Junction Temperature (T_j)	150 °C	175 °C
Reverse Recovery Charge (Q_{rr})	0 μC	0.39 μC
Package Stray Inductance (L_σ)	0.4 nH	7 nH
Device Package	GaN_{PX}	TO220-3

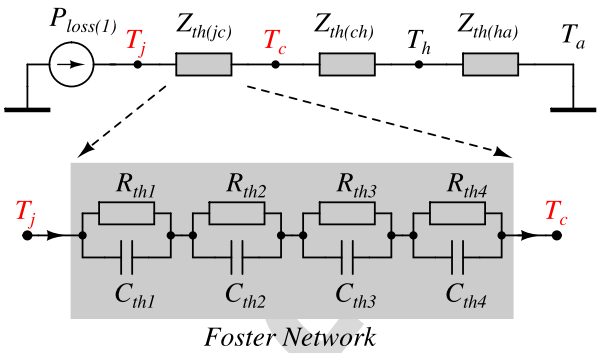

Fig. 3. Thermal model of a single power device, where the *RC* layer number is related to the device packaging technology, as shown in Table III.

TABLE III
THERMAL PARAMETERS FOR Si IGBT, Si DIODE, AND GaN HEMT

Impedance i		$Z_{th(j-c)}$ 1	2	3	4
Si IGBT	R_{thi} [°K/W]	0.07041042	0.3070851	0.3198984	0.1871538
	τ_i [s]	0.000096	0.00068	0.01084623	0.06925485
Si Diode	R_{thi} [°K/W]	0.4398	0.6662	0.4734	0.3169
	τ_i [s]	0.00013	0.0011	0.0071	0.04629
GaN HEMT	R_{thi} [°K/W]	0.05	-	-	-
	τ_i [s]	0.00025	-	-	-

or Si MOSFETs. At the 600 V blocking class, superjunction (SJ) Si MOSFETs can be an alternative to WBG devices, where a unipolar current conduction must be employed due to the poor body-diode characteristic of SJ devices [38], [39]. Since the 3L-ANPC inverter requires bipolar current condition, the comparison is limited to IGBT in Si-based devices in this paper. Device properties of the selected GaN HEMT and Si IGBT are presented in Table II. Both devices are at the 600 V blocking class and suitable for full bridge topologies with 400 V dc-link or multilevel topologies with 800 V dc link with the grid voltage of 230 V_{rms}. As it can be seen in Table II, the Si IGBT continuous current rating is almost equal to the rating of GaN HEMT device at 100 °C, and therefore, a fair comparison can be conducted between the two device technologies. Si IGBT switching losses are expected to be higher than GaN HEMTs. Regarding on-state losses, the GaN HEMT has better conduction performance in comparison with Si IGBT at lower case temperatures. The on-state performances of two technologies are presented in Table II. It can be seen that the variation of on-state performance of GaN HEMT is more sensitive to junction temperature increase in comparison with Si IGBT. Furthermore, it is shown in Table II that the device capacitance and reverse recovery characteristics of the GaN HEMTs are excellent in comparison with those of the Si IGBTs in the switching dynamics. This switching loss difference has an impact on the device loss distribution, which will be presented in simulations (Section III), as only two devices out of six in the 3L-ANPC leg are subject to switching losses.

In addition to the electrical parameters in Table II, it should be noted that the GaN HEMT device is packaged in a novel structure called GaN_{PX}. The package integrates and encapsulates the GaN HEMT die into a very thin (0.45 mm total thickness) high-temperature fiberglass matrix. Copper micro vias are used for vertical connections to facilitate heat transfer from the top side and electrical connections from the bottom side of the package. The GaNPX technology eliminates bond wires and solders joints, and achieves extremely low stray inductance [40]. As shown in Table II, the stray inductance of the GaN HEMT package has 17.5× less stray inductance per device than that of the Si IGBT package, relying on manufacturer information. This is a key aspect for drawing the maximum benefit from the WBG power devices. In addition, by using thick redistribution layer and copper on top of the die, competitive thermal impedance can be ensured.

Nevertheless, the thermal loading of the power electronic devices is still the major lifetime affecting factor, which is an essential part for reliability analysis. Hence, a thermal model of a single device is shown in Fig. 3. The device thermal network consists of thermal impedances between device junction and device case [$Z_{th(jc)}$], case and heat sink [$Z_{th(ch)}$], and heat sink and ambient [$Z_{th(ha)}$]. Based on manufacturer datasheets and SPICE models, Foster network parameters for junction-to-case impedance are presented in Table III. Obtained Foster network parameters are transferred to the Cauer network in the simulation environment for accurate thermal modeling. In the case of the GaN device, due its comparatively small dimensions, a satisfactory thermal description was achieved with only one *RC* group, whereas three groups have been used for the larger device and package types. Notably, the device thermal model is implemented along with the electrical model (see Fig. 1) in order to obtain the thermal performance with respect to converter instantaneous loading conditions, which are highly dependent on the solar and ambient temperature profiles and in return affect the semiconductor switch properties. One important aspect to consider for GaN HEMTs is the insulation of thermal pad of the device from heat sink, where common heat sink is used for the inverter and dc/dc converter. As the thermal pad of GaN HEMTs is directly connected to the substrate and source of the device internally, electrical isolation has to be provided in common heatsink applications. The thermal pad area of GaN HEMT is 20.5 mm^2

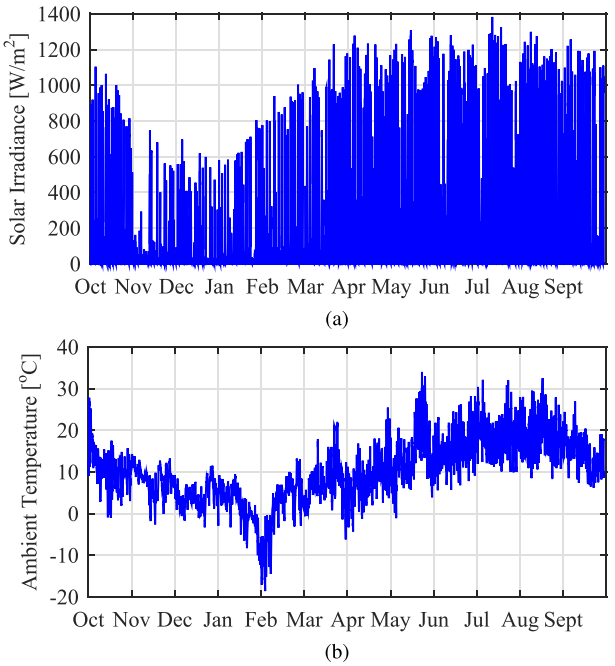

Fig. 4. Annual mission profile used in this paper. (a) Solar irradiance. (b) Ambient temperature profile in Aalborg.

and with a commercial thermally conductive insulator, which has 3.5 W/m.K thermal conductivity, 0.3 mm thickness, and 4-kV breakdown voltage [41]. Thus, an additional thermal resistance of 4 K/W is added to $Z_{\text{th(ch)}}$ in Fig. 3. The additional thermal resistance from the insulator increases the junction temperature of devices significantly due to the thermal pad size even at low switching frequencies. For Si IGBTs, thermally conductive insulator with 0.57 K/W thermal resistance and 4-kV breakdown voltage is considered for the isolation of discrete devices from common heat sink [42]. The common heat sink for the devices is modeled as a simple *RC* circuit. There are two reasons for this simplification.

1) The analysis in this paper focuses on the thermal profile analysis of steady-state device junction temperature and the heat sink will not have significant effect on thermal loading comparison.
2) The simplification of heat sink model leads to the acceleration of long-term mission profile simulations. Junction temperature comparisons with and without insulator will be presented over an annual mission profile by simulations in Section III.

D. Mission-Profile-Based Simulation

It is necessary to evaluate the performance of power electronic systems in long-term operation along with short-term operation, as the long-term operation profiles can have significant impact on efficiency, reliability, and lifetime of the entire system [25]. For short-term evaluation, the time-based simulation tools or prototype-based experiments can be conducted to assess the performance, but both of these approaches are not suitable for long-term evaluation due to the constraints of time, computational, and financial resources. Therefore, an efficient method is required to evaluate the long-term performance (see Figs. 5 and 7) [25], [26]. The long-term

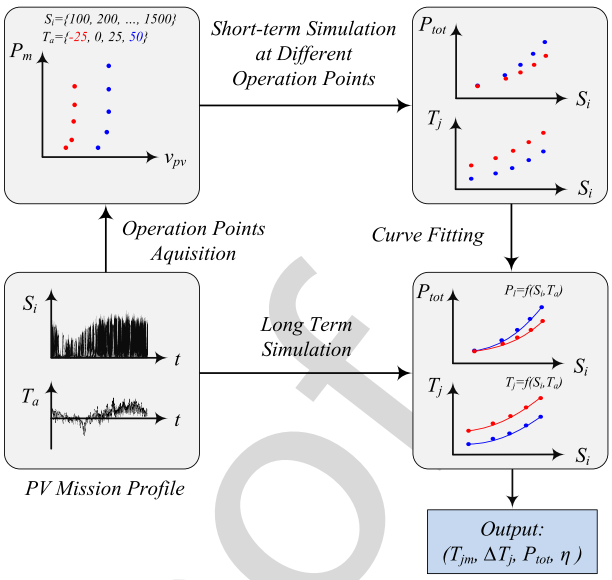

Fig. 5. Realization of the long-term mission profile-based analysis approach.

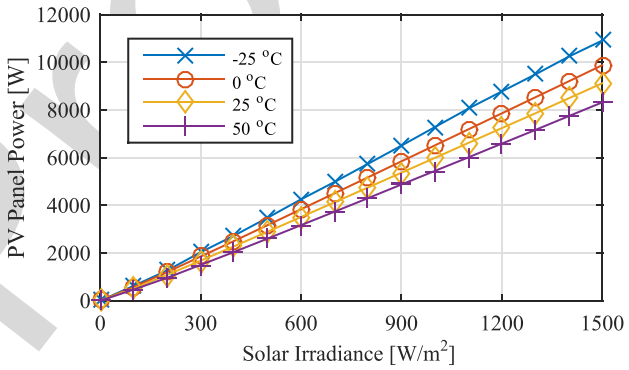

Fig. 6. PV panel output power with respect to solar irradiance and ambient temperature.

PV mission profile consists of solar irradiance level (S_i) and ambient temperature (T_a). In this paper, a real-field annual PV mission profile data (i.e., solar irradiance level and ambient temperature) in Aalborg is considered. The measured annual solar irradiance and ambient temperature data are shown in Fig. 4.

Realization of the long-term mission profile-based analysis is shown in Fig. 5. The first step of this analysis is to obtain the maximum power (P_m) operation points with respect to the PV module output voltage (v_{pv}) for the PV string specified in Table I, based on the measured different solar irradiance (S_i) and ambient temperature (T_a). Then, maximum power and operation voltage are fed into the short-term simulation model in order to obtain power loss (P_{tot}) and temperature profile (T_j) for each switching device in correspondence to an individual operation point (e.g., $P_m = 6$ kW and $V_{\text{pv}} = 400$ V for the case of 25 °C and 1000 W/m^2). The maximum output power of the PV panel with respect to solar irradiance and ambient temperature is shown in Fig. 6. The losses and temperature performance are finally curve-fitted with respect to the entire solar irradiance and ambient temperature spectrums in such a way to link a specific mission profile with the power electronic converter (electrical behavior). It should be pointed out here

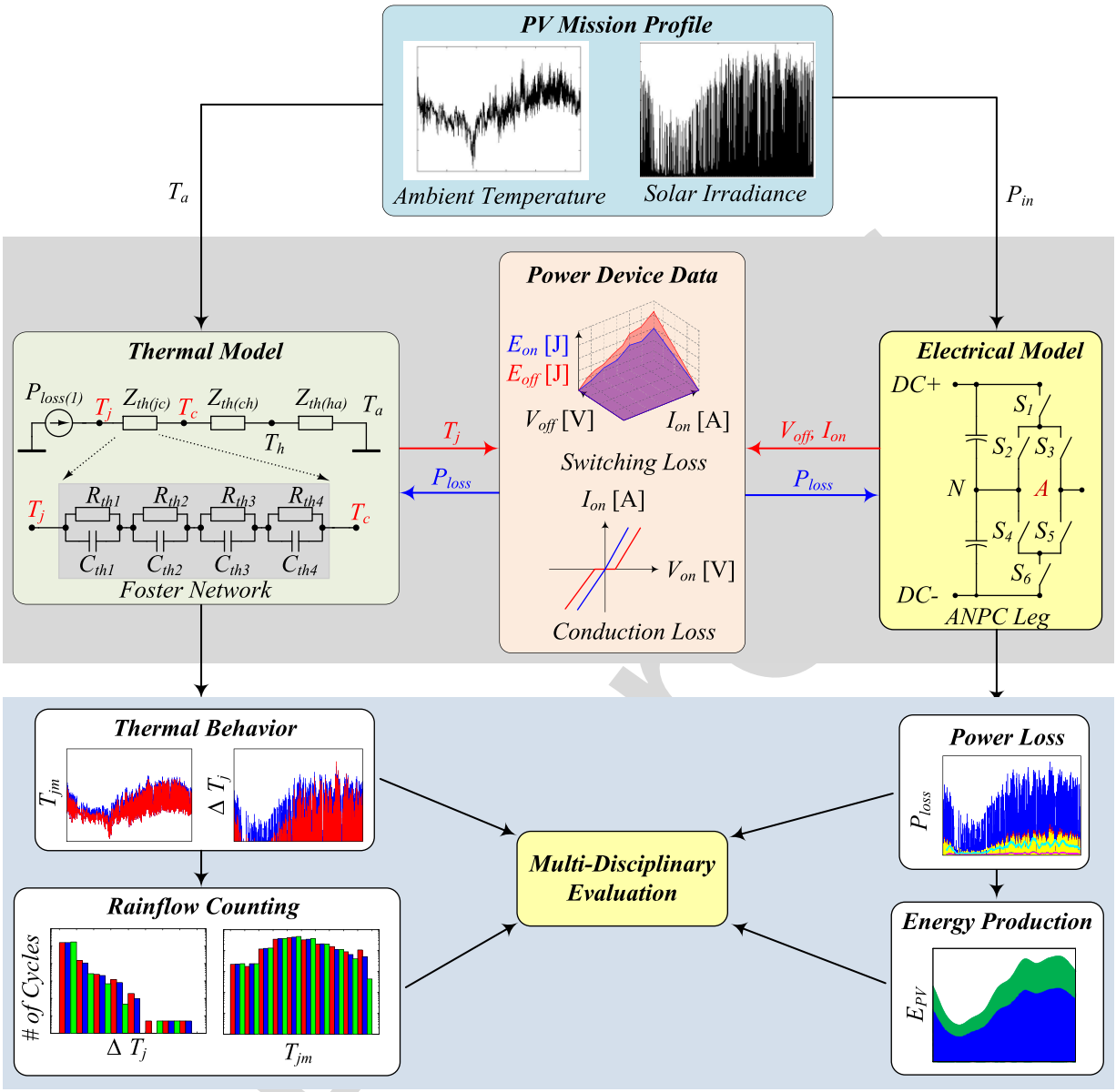

Fig. 7. Multidisciplinary analysis method.

that the MPPT control (dc–dc converter) efficiency has been assumed to 99%, since the focus of this paper is not on the MPPT control.

The detailed structure of the multidisciplinary analysis method is shown in Fig. 7. Short-term simulation model consists of two domains: thermal model and electrical model, which are linked via power device model. Electrical parameters affecting conduction and switching losses are fed to the power device model along with junction temperature from the thermal model in order to calculate power device losses with respect to predefined switching and conduction performance data. Then, the calculated power loss is fed to thermal model in order to recalculate the junction temperature and to the electrical model for the calculation of the total converter losses. This bidirectional data exchange between different simulation domains provide results that can be used for better understanding the thermal and electrical performances, enabling the multidisciplinary evaluation of the implemented modulation scheme, power devices, and converter topologies. Power device data can be obtained from detailed device datasheets that provide switching and conduction loss performances or double pulse tests.

III. Simulation Results

The simulations based on the approach explained in detail in Section II are carried out on a single-phase 3L-ANPC inverter with the assumption of a balanced three-phase grid system and operation. In this case, the analysis results can be extended to the three-phase 3L-ANPC converter shown in Fig. 1. Input power, total conduction losses, and total switching losses are recorded for converter performance evaluation according to the multidisciplinary approach. In addition to this, power losses,

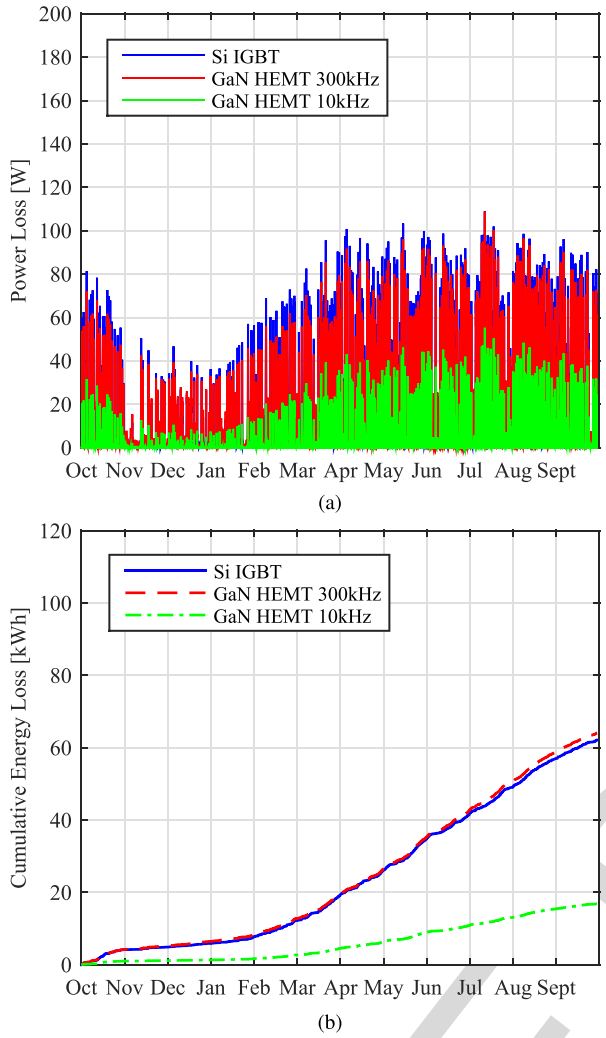

Fig. 8. Estimated annual power losses and cumulative energy loss of the ANPC inverter based on different technologies using the mission-profile analysis approach. (a) Annual power losses. (b) Cumulative energy losses.

mean, and maximum junction temperatures for each device are recorded for device in order to evaluate the loss distribution, thermal stress, and behavior of each power switch in a single 3L-ANPC leg. In the beginning of this section, overall inverter performance is presented, including inverter loss breakdown, annual power loss, and cumulative energy loss, for IGBT and GaN-based scenarios. These results are followed by the thermal stress comparison of each power device, including the power loss distribution, mean junction temperature, and junction temperature variation, for most stressed devices in the specific configuration.

A. Overall Power Loss and Energy Generation

The annual power loss and cumulative energy loss of three-phase 3L-ANPC inverter with Si IGBTs at 10 kHz, and with GaN HEMTs at 10 and 300 kHz are shown in Fig. 8. As it is expected from the results presented in the literature, the GaN-based 3L-ANPC inverter has a higher efficiency, and therefore less power losses throughout the year in comparison with those of the Si IGBT-based 3L-ANPC inverter. The cumulative energy loss for the Si IGBT-based inverter is around 64.1 kWh, and in contrast, for the GaN-based inverter at 10 and 300 kHz is 16.8 and 63.9 kWh, respectively. At the switching frequency of 300 kHz, although the GaN HEMTs are switched 30 times more than Si IGBTs, the associated additional energy losses due to the increased switching frequency are 74% of the total energy losses of the Si IGBT-based inverter. The average electricity price in Denmark for household consumers is 0.304 €/kWh [43]. Without considering thermal benefits of reduced converter losses, if the feed-in tariff is assumed to be the same as the utility tariff, it can be concluded that the GaN HEMT-based inverter at 10 kHz will bring additional €30.73 to the owner in comparison with the Si IGBT-based inverter. At 300 kHz, the GaN HEMT-based inverter will not bring significant operation income to the owner, whereas will provide reduction in initial system cost saving due to the reduction in cooling and output filtering requirements [20].

Conduction loss breakdown and switching loss breakdown of the Si and GaN-based inverter phase leg are shown in Fig. 9 with respect to four different ambient temperatures and at maximum solar irradiance for the given ambient temperature profile. At 10-kHz switching frequency, the conduction losses are dominating the overall converter losses for the Si IGBTs. Meanwhile, the losses reduce with respect to the temperature increase due to the reduction in the input power and relatively small temperature dependence of conduction performance of Si IGBTs at low collector current levels, as shown in Table II, despite the fact that the switching losses increase according to ambient temperature. On the other hand, the switching losses of the GaN HEMT-based inverter leg is negligible at 10 kHz, and the total losses are dominated by the conduction losses. The switching losses increase as the switching frequency is moved from 10 to 300 kHz in Fig. 9(b) and (c), but the overall losses of the phase leg is close to Si IGBT-based inverters, as it is shown in Fig. 9(a).

As the size of heat sink volume is inversely proportional to required thermal resistance $Z_{\text{th(ch)}}$ [20], [37], the heat sink volume of the GaN HEMT-based inverter at 300 kHz will still be smaller than that in the case of the Si-based inverter. Therefore, heat sink can still contribute to system level cost saving for the GaN-based inverter at a very high switching frequency.

B. Thermal Stress Comparison

The applied modulation scheme in Fig. 2 provides low conduction losses with the penalty of uneven loss distribution in the 3L-ANPC phase leg at unity power factor operation. During positive half cycle of the output voltage, S_1 is subject to hard switching and also conducts during active state, while S_3 conducts during positive and zero states, and S_2 only conducts during zero states. Therefore, it is expected to see highest power losses across S_1 or S_3 switches depending on the device switching, conduction performance, and inverter switching frequency. The loss distributions for upper devices in the 3L-ANPC - phase leg-A in Fig. 1 are shown in Fig. 10 for Si and GaN. In the Si-based inverter, due to the unity

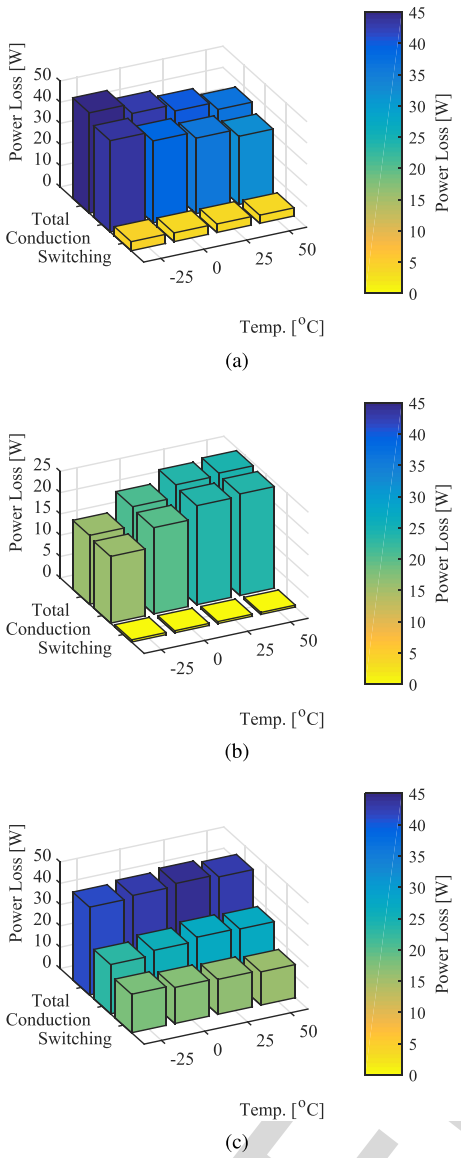

Fig. 9. Semiconductor total, conduction, and switching losses per phase leg of the ANPC inverter based on (a) Si IGBT technology with a switching frequency of 10 kHz, (b) GaN technology with a switching frequency of 10 kHz, and (c) GaN technology with a switching frequency of 300 kHz, where different ambient temperatures with the maximum solar irradiance level are considered.

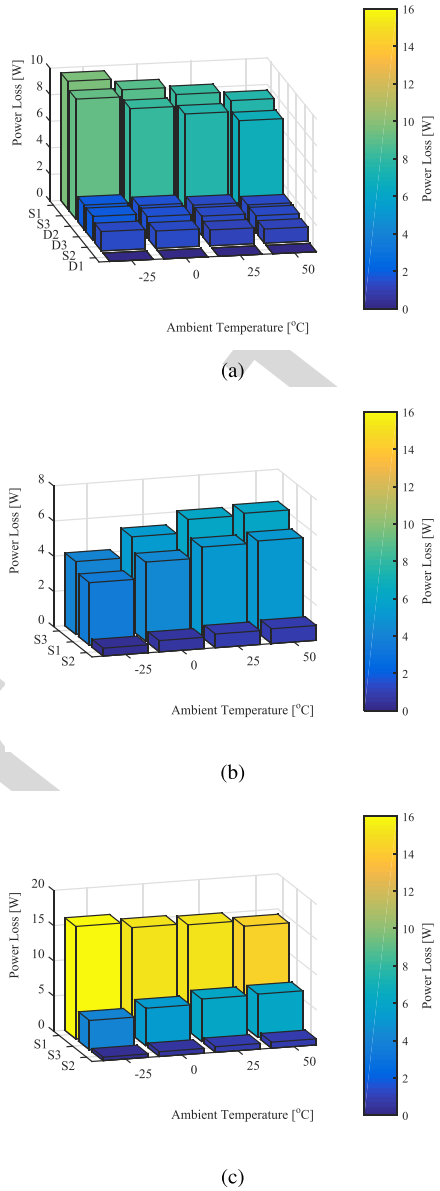

Fig. 10. Loss distribution of the ANPC inverter based on (a) Si IGBT technology with a switching frequency of 10 kHz, (b) GaN technology with a switching frequency of 10 kHz, and (c) GaN technology with a switching frequency of 300 kHz, where different ambient temperatures with the maximum solar irradiance level are considered.

power factor operation, antiparallel diodes D_2 and D_3 only conduct during positive and negative zero states. Although S_3 has higher conduction losses than S_1, S_1 has the highest losses in the inverter leg due to the switching loss contribution shown in Fig. 9(a). On the other side, for the GaN-based inverter at 10 and 300 kHz in Fig. 10(b) and (c), the loss distributions among S_1 and S_3 vary with respect to the selected switching frequency. High switching performance of the GaN HEMTs shows the impact at 10 kHz by keeping the power losses of S_1 less than S_3. By increasing the switching frequency to 300 kHz, switching losses become significant in overall losses [Fig. 9(c)], resulting in that S_1 has the highest power loss in the inverter leg.

As the devices with highest power losses and, therefore, the thermal stress in each configuration are identified, further thermal performance analysis can be conducted on these devices based on the annual mission profile. Mean junction temperature (T_j) and junction temperature variation (ΔT_j) for devices with the highest thermal stress are shown in Fig. 11(a) and (b), respectively. Mean junction temperature of S_1 in a Si IGBT-based inverter is <50 °C, while the mean junction temperature of S_1 in the GaN HEMT-based inverter with 300 kHz switching frequency can go up to 75 °C during summer time. The mean junction temperature follows the ambient temperature trend throughout the year and can show significant variations based on the solar irradiance and ambient temperature. Regarding the junction temperature variations, S_1 in a GaN HEMT inverter with 300 kHz has the highest

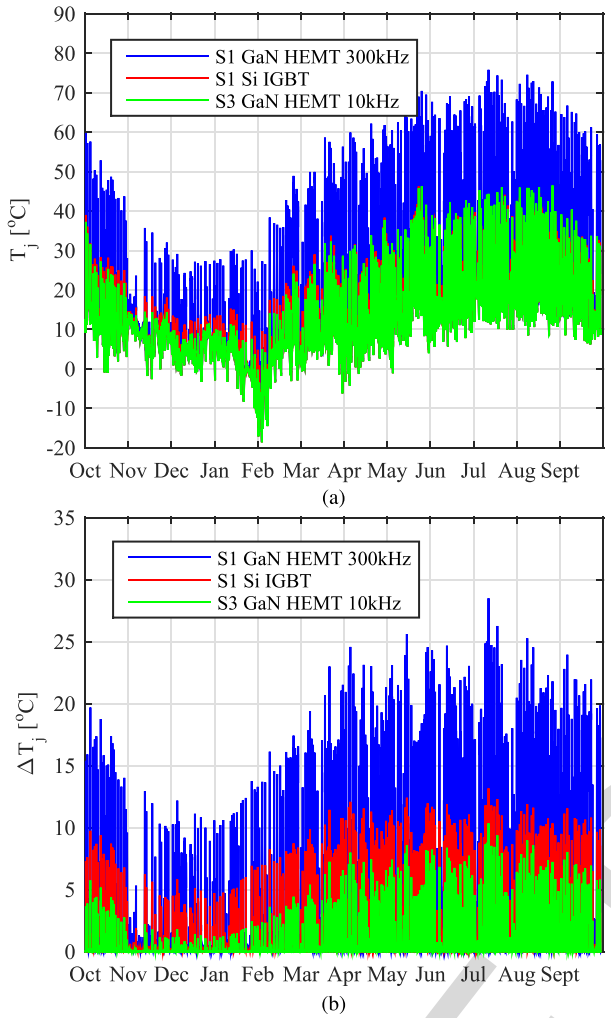

Fig. 11. Thermal loading profiles for the most stressed devices in 3L-ANPC inverter through a year. (a) Mean junction temperature. (b) Junction temperature variation.

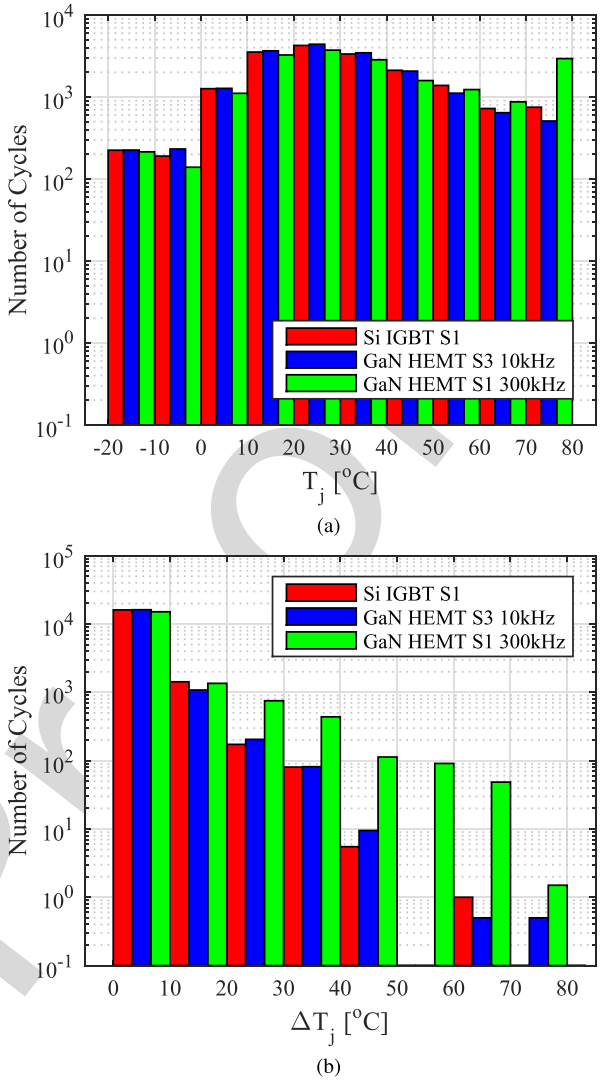

Fig. 12. Rainflow counting results for the thermal loading profiles shown in Fig. 12 under a yearly mission profile. (a) Mean junction temperature. (b) Cycle amplitude.

temperature variation across the junction of the device. S_3 in a GaN HEMT inverter at 10 kHz has a similar performance during warm months to that of $S1$ in a Si IGBT inverter due to the increased conduction losses.

It can be seen from Fig. 12 that the long-term mean junction temperature and junction temperature fluctuations are irregular profiles with varying frequencies and amplitudes. In order to make the results more meaningful, cycling counting methods can be applied to the mean junction temperature and junction temperature variation data. The number of cycles at each temperature level is dependent to mission profile, thermal, and electrical models as it is explained in the Section II. Rainflow is one of the cycle-counting methods to identify full and half cycles within irregular profiles, and is chosen in this paper. It has been used in the calculation of lifetime of power modules based on device solder temperature profiles [44]. The histograms of mean junction temperature (T_j) and junction temperature variations (ΔT_j) presented for the most stressed devices are shown in Fig. 12(a) and (b), respectively. Replacing Si IGBTs with GaN HEMTs at 10-kHz switching frequency reduces the number of cycles of at higher temperatures. On the other hand, the GaN HEMTs with 300-kHz switching frequency have increased T_j and ΔT_j at higher temperatures, which means that the device is subject to higher thermal stresses in comparison with other two options.

The Coffin–Manson model for the conventional power modules indicates that the number of failures in a power module is only dependent on the temperature cycles, cycle amplitude ΔT_j, and mean junction temperature T_j [45]. Therefore, with adequate device packaging models for the GaN HEMTs and Si IGBTs, lifetime consumption of the power devices at different switching frequencies can be calculated, and then, an optimization between reliability, efficiency, and system volume can be achieved.

C. Thermal Interface Material Impact on GaN HEMT

As it is mentioned earlier, the thermally conductive insulator [thermal interface material (TIM)] with 4 K/W thermal resistance has been placed between the thermal pad of the GaN HEMT and the heat sink. As the junction-to-case

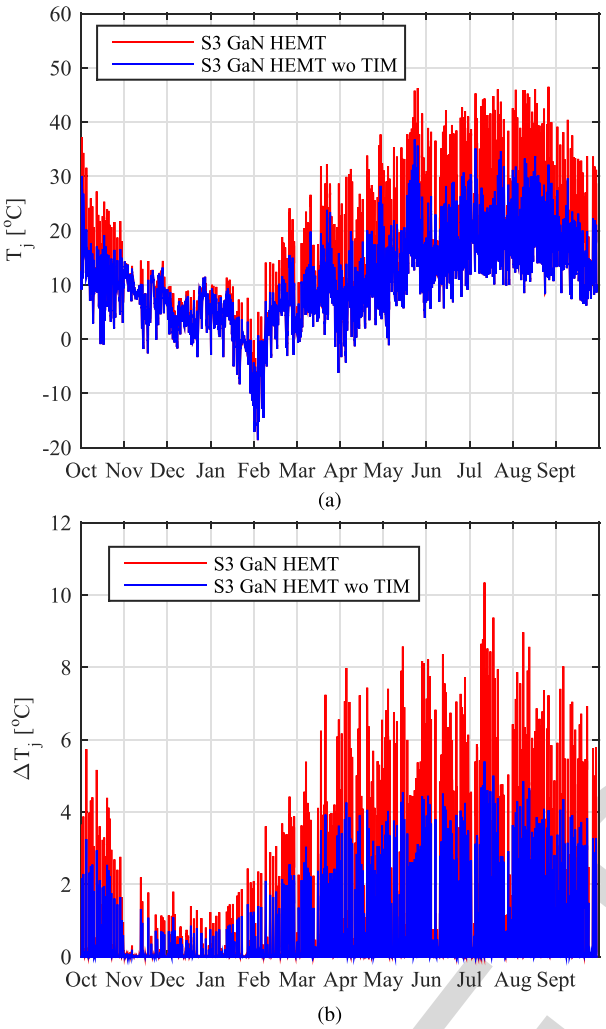

Fig. 13. Thermal loading of the S_3 GaN HEMT in the 3L-ANPC inverter with and without electrical insulation (TIM) material. (a) Mean junction temperature. (b) Junction temperature variation.

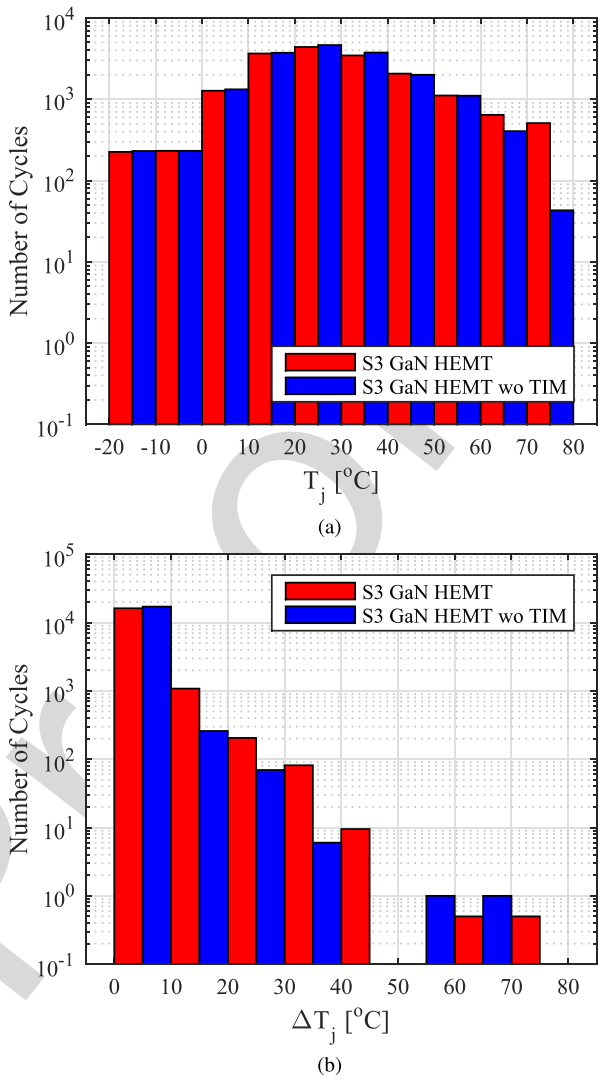

Fig. 14. Rainflow counting results of the thermal loading profile shown in Fig. 13 (for the S_3 GaN HEMT device) with and without electrical insulation material. (a) Mean junction temperature. (b) Junction temperature variations.

thermal resistance of GaN HEMTs is extremely low, the thermal resistance of TIM will increase the thermal stress across the GaN power devices. In order to illustrate this, the mean junction and junction temperature variation of S_3 in a GaN HEMT inverter at 10-kHz switching frequency with and without TIM are shown in Fig. 13. It is clear that the mean temperature can increase by 10 °C during warm days and the maximum junction temperature variation can increase from 5 °C to 10 °C. The histograms based on mean junction temperature and junction temperature variations in Fig. 13 are shown in Fig. 14(a) and (b), respectively. The histogram results show that the number of cycles for mean junction temperature and junction temperature variation is higher with TIM. Therefore, innovative cooling solutions are required for the GaN packages that provide excellent electrical isolation without compromising the thermal performance of the devices.

IV. Experimental Results

The performance of 600 V Si IGBTs has been well studied in the literature for different applications, and some these results have been discussed in Section I. On the other hand, normally off 650 V GaN HEMTs with low inductance package recently emerged for power electronic applications. Therefore, a GaN HEMT-based single-phase ANPC inverter demonstrator has been designed and built. The performance of GaN HEMT devices is experimentally evaluated and presented in this section.

The GaN HEMT-based single-phase ANPC inverter is shown in Fig. 15. The power cell is formed by four-layer PCB with 140 μm copper on each layer. The power cell consists of high-frequency dc-link capacitors, GaN HEMT switches, gate drivers, signal and power isolation circuits for gate drivers, and fiber optic receivers for gate signals. The S_1–S_3 GaN devices are placed on the top side of the PCB, while S_4–S_6 GaN devices are placed on the bottom side of the PCB in symmetry to S_1–S_3 for minimized commutation loop and high switching speed. The PCB is designed to have a modular system with the option to extend the demonstrator to three phase by stacking PCBs vertically. Regarding cooling

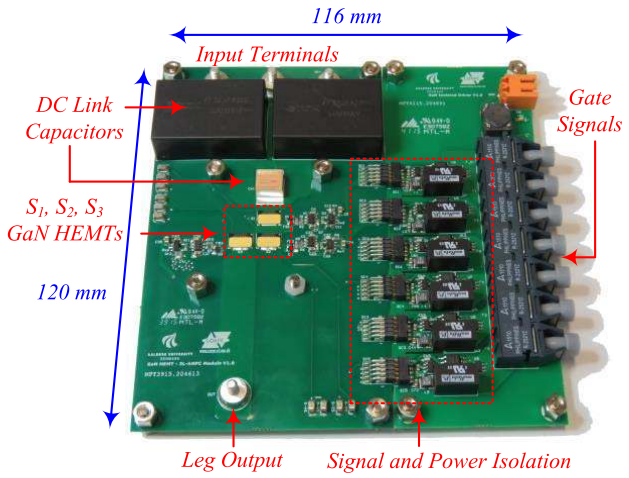

(a)

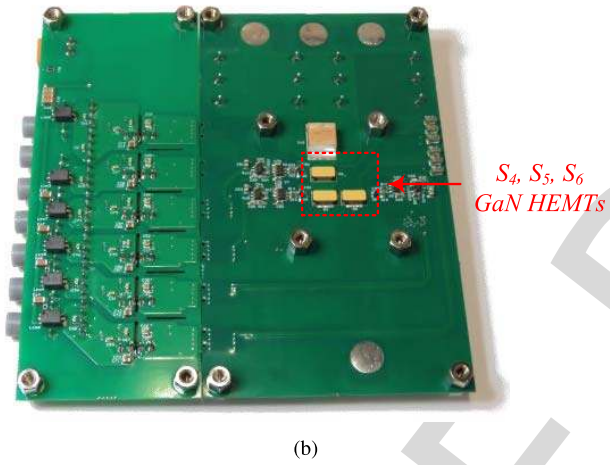

(b)

Fig. 15. Hardware of the GaN HEMT-based single-phase ANPC power cell. (a) Top view. (b) Bottom view.

of power switches, two commercial heat sinks, which are joined by four screws with compression springs in order to apply equal contact pressure to the devices from top to bottom part of the PCB. The PCB has been presented without heat sinks in order to show the device positions on the board.

A. Switching Performance

The ANPC power cell is initially operated as a buck dc/dc converter in order to evaluate the switching performance of GaN devices and designed power cell. For buck configuration, upper switches S_1–S_3 are used, where S_3 is completely on during the switching period and complementary gate signals are applied to S_1 and S_2 with 200-ns dead time.

The switching waveforms at 40-kHz switching frequency with 400 V dc-link voltage and 1-kW output power are shown in Fig. 16. In Fig. 16(b), the output current commutates from S_2 to S_1 and S_1 is subject to hard switching. The commutation from S_1 to reverse conduction of S_2 is shown in Fig. 16(c).

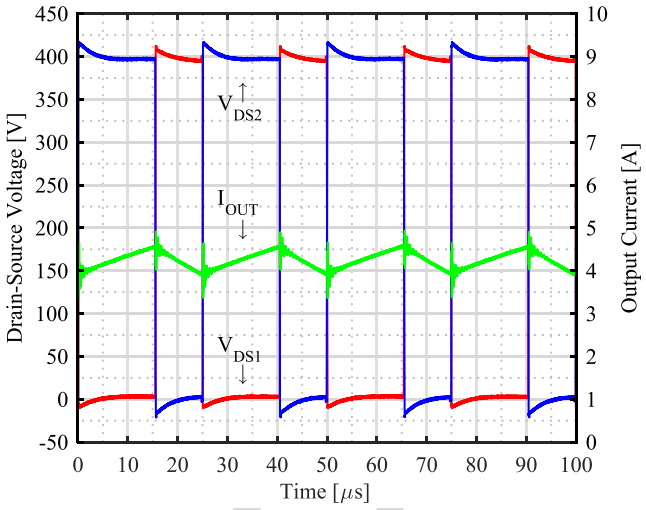

(a)

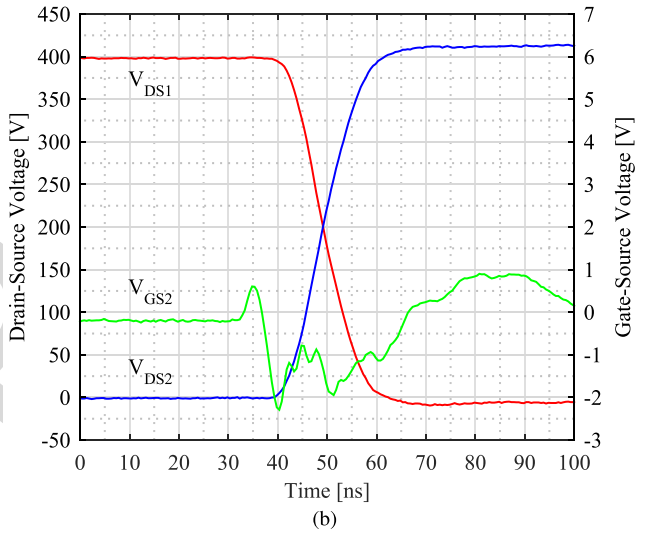

(b)

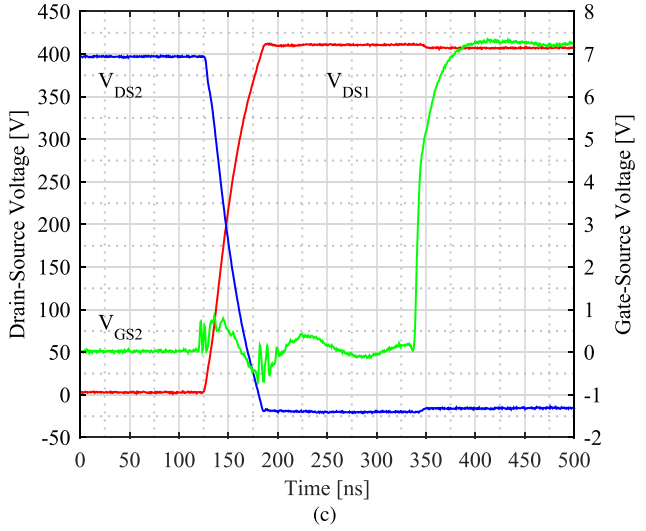

(c)

Fig. 16. Switching performance of the GaN HEMT in the 3L-ANPC inverter. (a) Device voltage and output current, (b) hard commutation, and (c) soft commutation waveforms with buck configuration.

Drain–source voltage waveforms V_{DS1} and V_{DS2} prove high switching speed of GaN HEMTs with 13.2-ns rise and fall time of V_{DS2} and V_{DS1}, respectively.

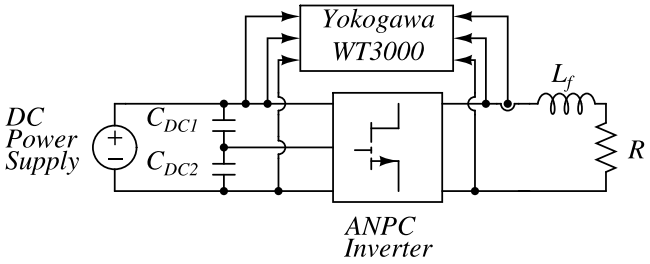

Fig. 17. Inverter test setup.

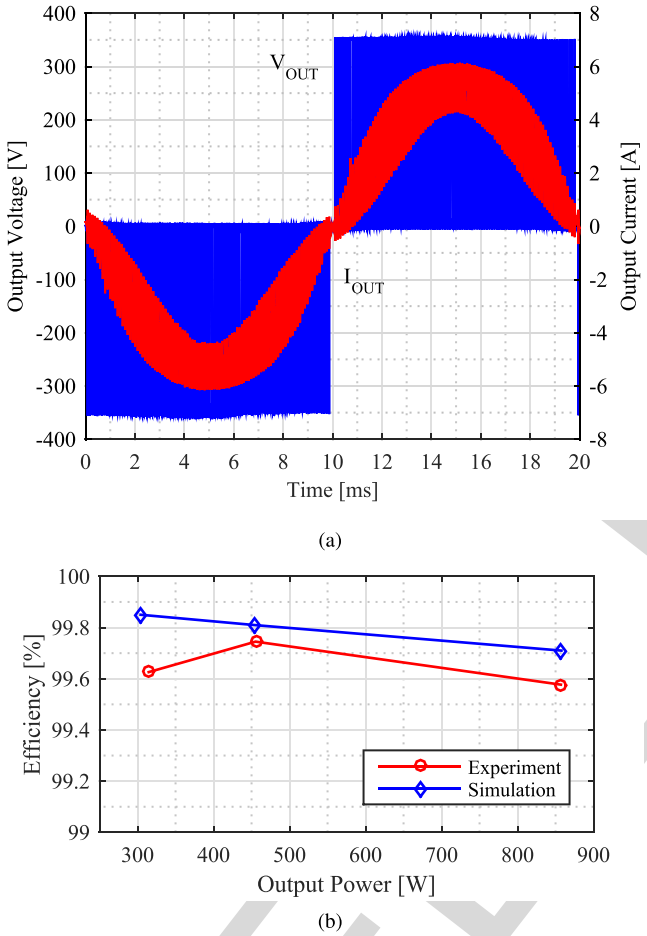

Fig. 18. (a) Experimental output voltage and current waveforms at 800-W output power. (b) Efficiency of the 3L-ANPC power cell with experimental and simulation results.

B. Inverter Performance

The single-phase 3L-ANPC inverter prototype in Fig. 15 is tested with 700 V dc link and 10-kHz switching frequency to demonstrate the performance of GaN-based power cell without heat sink. The inverter test setup is shown in Fig. 17. The inverter is powered by a dc power supply with dc-link decoupling capacitors. An *RL* load configuration is used for the evaluation of performance under different load conditions. Efficiency and losses of power cell are measured by Yokogawa WT3000E precision power analyzer with 0.01% power accuracy.

The experimental output current and voltage waveforms, and power cell efficiency with experimental and simulation results are shown in Fig. 18(a) and (b), respectively. The experimental results support the validity of high performance of GaN HEMT devices in simulation and comparison with Si IGBTs. The efficiency comparison in Fig. 18(b) validates the performance assumption of GaN HEMTs in the inverter operation mode.

V. Conclusion

This paper has explored the challenging issues and the possibility of moving to new technologies, namely, GaN HEMTs in PV inverters, with special focus on the reliability and thermal performance. A comparison of Si IGBT against GaN HEMT with three different possibilities: 1) with TIM at 10 kHz; 2) without TIM at 10 kHz; and 3) with TIM at 300 kHz has been performed. Considering a long-term mission profile, the results suggest higher reliability expectation for GaN HEMTs at low frequencies due to considerably lower power losses and thermal resistance between junction and heat sink, whereas TIM has contributed to significant additional thermal stress. Experimental results of single-phase inverter prove the high performance of GaN HEMT devices. The results in this paper are fundamental to confidently predict the lifetime of novel GaN-based PV inverters considering long-term mission profiles.

Acknowledgment

The authors would like to thank G. Haynes from GaN Systems for constructive discussions and providing detailed data about GaN HEMT devices.

References

[1] *Global Market Outlook For PV Until 2018*, Eur. Photovoltaic Ind. Assoc., Brussels, Belgium, 2014.

[2] S. B. Kjaer, J. K. Pederson, and F. Blaabjerg, "A review of single-phase grid-connected inverters for photovoltaic modules," *IEEE Trans. Ind. Appl.*, vol. 41, no. 5, pp. 1292–1306, Sep./Oct. 2005.

[3] J. M. Carrasco *et al.*, "Power-electronic systems for the grid integration of renewable energy sources: A survey," *IEEE Trans. Ind. Electron.*, vol. 53, no. 4, pp. 1002–1016, Jun. 2006.

[4] D. Meneses, F. Blaabjerg, O. García, and J. A. Cobos, "Review and comparison of step-up transformerless topologies for photovoltaic AC-module application," *IEEE Trans. Power Electron.*, vol. 28, no. 6, pp. 2649–2663, Jun. 2013.

[5] T. Kerekes, R. Teodorescu, P. Rodríguez, G. Vázquez, and E. Aldabas, "A new high-efficiency single-phase transformerless PV inverter topology," *IEEE Trans. Ind. Electron.*, vol. 58, no. 1, pp. 184–191, Jan. 2011.

[6] E. Gubía, P. Sanchis, A. Ursúa, J. López, and L. Marroyo, "Ground currents in single-phase transformerless photovoltaic systems," *Prog. Photovolt., Res. Appl.*, vol. 15, no. 7, pp. 629–650, Nov. 2007.

[7] J. Millan, P. Godignon, X. Perpina, A. Perez-Tomas, and J. Rebollo, "A survey of wide bandgap power semiconductor devices," *IEEE Trans. Power Electron.*, vol. 29, no. 5, pp. 2155–2163, May 2014.

[8] C. Wilhelm, D. Kranzer, and B. Burger, "Development of a highly compact and efficient solar inverter with silicon carbide transistors," in *Proc. 6th Int. Conf. Integr. Power Electron. Syst. (CIPS)*, 2010, pp. 1–6.

[9] B. Burger and D. Kranzer, "Extreme high efficiency PV-power converters," in *Proc. 13th Eur. Conf. Power Electron. Appl. (EPE)*, 2009, pp. 1–13.

[10] D. Kranzer, C. Wilhelm, F. Reiners, and B. Burger, "Application of normally-off SiC-JFETs in photovoltaic inverters," in *Proc. 13th Eur. Conf. Power Electron. Appl. (EPE)*, Sep. 2009, pp. 1–6.

[11] D. Bergogne *et al.*, "Normally-on SiC JFETs in power converters: Gate driver and safe operation," in *Proc. 6th Int. Conf. Integr. Power Electron. Syst.*, Mar. 2010, pp. 1–6.

[12] E. Gurpinar, D. De, A. Castellazzi, D. Barater, G. Buticchi, and G. Francheschini, "Performance analysis of SiC MOSFET based 3-level ANPC grid-connected inverter with novel modulation scheme," in *Proc. IEEE 15th Workshop Control Modeling Power Electron. (COMPEL)*, Jun. 2014, pp. 1–7.
[13] D. De, A. Castellazzi, A. Solomon, A. Trentin, M. Minami, and T. Hikihara, "An all SiC MOSFET high performance PV converter cell," in *Proc. 15th Eur. Conf. Power Electron. Appl. (EPE)*, Sep. 2013, pp. 1–10.
[14] D. Barater, C. Concari, G. Buticchi, E. Gurpinar, D. De, and A. Castellazzi, "Performance evaluation of a 3-level ANPC photovoltaic grid-connected inverter with 650 V SiC devices and optimized PWM," in *Proc. IEEE Energy Convers. Congr. Expo. (ECCE)*, Sep. 2014, pp. 2233–2240.
[15] A. Hensel, C. Wilhelm, and D. Kranzer, "Application of a new 600 V GaN transistor in power electronics for PV systems," in *Proc. 15th Int. Power Electron. Motion Control Conf. (EPE/PEMC)*, Sep. 2012, pp. DS3d.4-1–DS3d.4-5.
[16] T. Ueda, "Recent advances and future prospects on GaN-based power devices," in *Proc. Int. Power Electron. Conf. (IPEC-ECCE ASIA)*, Hiroshima, Japan, May 2014, pp. 2075–2078.
[17] T. Morita *et al.*, "99.3% efficiency of three-phase inverter for motor drive using GaN-based gate injection transistors," in *Proc. 26th Annu. IEEE Appl. Power Electron. Conf. Expo. (APEC)*, Mar. 2011, pp. 481–484.
[18] A. Tüysüz, R. Bosshard, and J. W. Kolar, "Performance comparison of a GaN GIT and a Si IGBT for high-speed drive applications," in *Proc. Int. Power Electron. Conf. (IPEC-ECCE ASIA)*, Hiroshima, Japan, May 2014, pp. 1904–1911.
[19] E. Gurpinar and A. Castellazzi, "SiC and GaN based BSNPC inverter for photovoltaic systems," in *Proc. 17th Eur. Conf. Power Electron. Appl. (EPE ECCE-Europe)*, Sep. 2015, pp. 1–10.
[20] E. Gurpinar and A. Castellazzi, "Single-phase T-type inverter performance benchmark using Si IGBTs, SiC MOSFETs and GaN HEMTs," *IEEE Trans. Power Electron.*, vol. 31, no. 10, Oct. 2016, doi: 10.1109/TPEL.2015.2506400.
[21] X. Huang, Z. Liu, Q. Li, and F. C. Lee, "Evaluation and application of 600 V GaN HEMT in cascode structure," *IEEE Trans. Power Electron.*, vol. 29, no. 5, pp. 2453–2461, May 2014.
[22] T. Ishibashi *et al.*, "Experimental validation of normally-on GaN HEMT and its gate drive circuit," *IEEE Trans. Ind. Appl.*, vol. 51, no. 3, pp. 2415–2422, May 2015.
[23] Y. Yang, P. Enjeti, F. Blaabjerg, and H. Wang, "Wide-scale adoption of photovoltaic energy: Grid code modifications are explored in the distribution grid," *IEEE Ind. Appl. Mag.*, vol. 21, no. 5, pp. 21–31, Sep./Oct. 2015.
[24] E. Koutroulis and F. Blaabjerg, "Design optimization of transformerless grid-connected PV inverters including reliability," *IEEE Trans. Power Electron.*, vol. 28, no. 1, pp. 325–335, Jan. 2013.
[25] Y. Yang, H. Wang, F. Blaabjerg, and K. Ma, "Mission profile based multi-disciplinary analysis of power modules in single-phase transformerless photovoltaic inverters," in *Proc. 15th Eur. Conf. Power Electron. Appl. (EPE)*, Sep. 2013, pp. 1–10.
[26] A. Anurag, Y. Yang, and F. Blaabjerg, "Thermal performance and reliability analysis of single-phase PV inverters with reactive power injection outside feed-in operating hours," *IEEE J. Emerg. Sel. Topics Power Electron.*, vol. 3, no. 4, pp. 870–880, Dec. 2015.
[27] N.-C. Sintamarean, F. Blaabjerg, H. Wang, F. Iannuzzo, and P. de Place Rimmen, "Reliability oriented design tool for the new generation of grid connected PV-inverters," *IEEE Trans. Power Electron.*, vol. 30, no. 5, pp. 2635–2644, May 2015.
[28] S. Kouro, J. I. Leon, D. Vinnikov, and L. G. Franquelo, "Grid-connected photovoltaic systems: An overview of recent research and emerging PV converter technology," *IEEE Ind. Electron. Mag.*, vol. 9, no. 1, pp. 47–61, Mar. 2015.
[29] T. Bruckner, S. Bernet, and H. Guldner, "The active NPC converter and its loss-balancing control," *IEEE Trans. Ind. Electron.*, vol. 52, no. 3, pp. 855–868, Jun. 2005.
[30] A. Nabae, I. Takahashi, and H. Akagi, "A new neutral-point-clamped PWM inverter," *IEEE Trans. Ind. Appl.*, vol. IA-17, no. 5, pp. 518–523, Sep. 1981.
[31] J. Rodriguez, S. Bernet, B. Wu, J. O. Pontt, and S. Kouro, "Multilevel voltage-source-converter topologies for industrial medium-voltage drives," *IEEE Trans. Ind. Electron.*, vol. 54, no. 6, pp. 2930–2945, Dec. 2007.
[32] T. Bruckner, S. Bernet, and P. K. Steimer, "Feedforward loss control of three-level active NPC converters," *IEEE Trans. Ind. Appl.*, vol. 43, no. 6, pp. 1588–1596, Nov. 2007.
[33] P. Barbosa, P. Steimer, J. Steinke, M. Winkelnkemper, and N. Celanovic, "Active-neutral-point-clamped (ANPC) multilevel converter technology," in *Proc. Eur. Conf. Power Electron. Appl.*, 2005, pp. P.1–P.10.
[34] D. Floricau, E. Floricau, and M. Dumitrescu, "Natural doubling of the apparent switching frequency using three-level ANPC converter," in *Proc. IEEE Int. School Nonsinusoidal Currents Compensation*, vol. 2. Jun. 2008, pp. 1–6, doi: 10.1109/ISNCC.2008.4627496.
[35] Y. Jiao, S. Lu, and F. C. Lee, "Switching performance optimization of a high power high frequency three-level active neutral point clamped phase leg," *IEEE Trans. Power Electron.*, vol. 29, no. 7, pp. 3255–3266, Feb. 2013.
[36] J. Mookken, B. Agrawal, and J. Liu, "Efficient and compact 50 kW Gen2 SiC device based PV string inverter," in *Proc. PCIM Eur., Int. Exhibit. Conf. Power Electron., Intell. Motion, Renew. Energy Energy Manage.*, May 2014, pp. 1–7.
[37] J.-I. Itoh and T. Araki, "Volume evaluation of a PWM inverter with wide band-gap devices for motor drive system," in *Proc. IEEE ECCE Asia Downunder*, Jun. 2013, pp. 372–378.
[38] P. Anthony and N. McNeill, "The efficient deployment of silicon super-junction MOSFETs as synchronous rectifiers," in *Proc. 7th IET Int. Conf. Power Electron., Mach. Drives (PEMD)*, Apr. 2014, pp. 1–6.
[39] M. Conrad and R. W. DeDoncker, "Avoiding reverse recovery effects in super junction MOSFET based half-bridges," in *Proc. IEEE 6th Int. Symp. Power Electron. Distrib. Generat. Syst. (PEDG)*, Jun. 2015, pp. 1–5.
[40] GaN Systems. *GaNPX Packaging*, accessed on May 1, 2016. [Online]. Available: http://www.gansystems.com/ganpx_packaging_new.php
[41] *Bergquist Sil-Pad 2000*, accessed on May 1, 2016. [Online]. Available: http://www.bergquistcompany.com/thermal_materials/sil_pad/sil-pad-2000_properties.htm
[42] *Bergquist Sil-Pad 2000, 2015-54 TO-220*, accessed on May 1, 2016. [Online]. Available: http://www.bergquistcompany.com/pdfs/dataSheets/PDS_SP_2000_0410.pdf
[43] *Energy Price Statistics—Statistics Explained*, accessed on May 1, 2016. [Online]. Available: http://ec.europa.eu/eurostat/statistics-explained/index.php/Energy_price_statistics
[44] M. Musallam and C. M. Johnson, "An efficient implementation of the rainflow counting algorithm for life consumption estimation," *IEEE Trans. Rel.*, vol. 61, no. 4, pp. 978–986, Dec. 2012.
[45] Y. Yang, H. Wang, and F. Blaabjerg, "Improved reliability of single-phase PV inverters by limiting the maximum feed-in power," in *Proc. IEEE Energy Convers. Congr. Expo. (ECCE)*, Sep. 2014, pp. 128–135.

Emre Gurpinar (S'11) received the B.Sc. degree in electrical engineering from Istanbul Technical University, Istanbul, Turkey, in 2009, and the M.Sc. degree in power electronics, machines, and drives from the University of Manchester, Manchester, U.K. in 2010. He is currently pursuing the Ph.D. degree with the University of Nottingham, Nottingham, U.K. He is involved in the Ph.D. thesis based on wide bandgap semiconductor-based renewable power converters.

He was a Visiting Ph.D. Student with the Department of Energy Technology, Aalborg University, Aalborg, Denmark, in 2015. He was a Research and Development Power Electronics Engineer with General Electric, Coventry?, U.K. His current research interests include wide bandgap power devices, high-frequency converters, renewable power systems, and hybrid multilevel inverters.

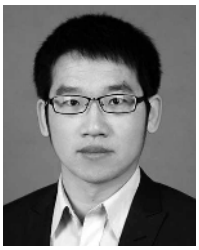

Yongheng Yang (S'12–M'15) received the B.Eng. degree from Northwestern Polytechnical University, Xi'an, China, in 2009, and the Ph.D. degree from Aalborg University, Aalborg, Denmark, in 2014.

He was a Post-Graduate with Southeast University, Nanjing, China, from 2009 to 2011. In 2013, he was a Visiting Scholar with the Department of Electrical and Computer Engineering, Texas A&M University, College Station, TX, USA. Since 2014, he has been with the Department of Energy Technology, Aalborg University, where he is currently an Assistant Professor. His current research interests include grid integration of renewable energy systems, power converter design, analysis and control, harmonics identification and mitigation, and reliability in power electronics.

Dr. Yang is a member of the IEEE Power Electronics Society Students and Young Professionals Committee, where he is responsible for the webinar series. He serves as a Guest Associate Editor of the IEEE JOURNAL OF EMERGING AND SELECTED TOPICS IN POWER ELECTRONICS of the Special Issue on Power Electronics for Energy Efficient Buildings. He has also been invited as a Guest Editor of *Applied Sciences* of the Special Issue on Advancing Grid-Connected Renewable Generation Systems. He is an active reviewer for relevant top-tier journals.

Francesco Iannuzzo (M'04–SM'12) received the M.Sc. degree in electronics engineering and the Ph.D. degree in electronic and information engineering from the University of Naples, Naples, Italy, in 1997 and 2001, respectively.

He was a Researcher with the University of Cassino, Cassino, Italy, from 2000 to 2006, where he became an Aggregate Professor in 2006 and has been an Associate Professor since 2012. In 2014, he was a Professor of Reliable Power Electronics with Aalborg University, Aalborg, Denmark, where he is part of the Center of Reliable Power Electronics. He is primarily specialized in power device modeling. He has authored or co-authored over 100 publications in journals and international conferences, and one patent on an innovative inverter topology for very compact, galvanic-isolated auxiliary power supply for heavy train applications. His current research interests include reliability of power devices, including cosmic rays, power device failure modeling, and testing of power modules up to Megawatt-scale under extreme conditions, such as overvoltage, overcurrent, overtemperature, and short circuit.

Prof. Iannuzzo is a Senior Member of the IEEE Reliability Society, the IEEE Electron Device Society, the IEEE Industrial Electronic Society, the IEEE Industry Application Society, and the Italian Electric, Electronic and Telecommunication Association. He was the Technical Program Committee Co-Chair in two editions of the European Symposium on Reliability and Failure analysis. He permanently serves as an Expert and a Peer Reviewer for several conferences and journals in Applied Power Electronics Conference, Energy Conversion Congress and Exposition, European Conference on Power Electronics and Applications, ESREF, IECON, *Elsevier Microelectronics Reliability*, the IEEE TRANSACTIONS ON INDUSTRIAL ELECTRONICS, the IEEE TRANSACTIONS ON INDUSTRIAL INFORMATICS, and the IEEE TRANSACTIONS ON POWER ELECTRONICS.

Alberto Castellazzi received the Laurea degree in physics from the University of Milan, Milan, Italy, in 1998, and the Ph.D. degree in electrical engineering from the Technical University of Munich, Munich, Germany, in 2004.

He has been active in power electronics research and development for over 15 years and has had extensive collaborations with major European and international industrial research laboratories and groups on publicly and privately funded research projects. He is currently an Associate Professor of Power Electronics with The University of Nottingham, Nottingham, U.K. He has authored or co-authored over 130 papers in peer reviewed specialist journals and conference proceedings, for which he also regularly acts as a Reviewer. His current research interests include characterization, modeling, application, packaging, and cooling of power devices.

Dr. Castellazzi is a member of the Technical Program Committee of the nternational Symposium on Power Semiconductor Devices and ICs, Electronics System-Integration Technology Conferences, and ECCE-Asia.

Frede Blaabjerg (S'86–M'88–SM'97–F'03) received the Ph.D. degree from Aalborg University, Aalborg, Denmark, in 1992.

He was with ABB-Scandia, Randers, Denmark, from 1987 to 1988. He became an Assistant Professor in 1992, an Associate Professor in 1996, and a Full Professor of Power Electronics and Drives in 1998. His current research interests include power electronics and its applications, such as in wind turbines, PV systems, reliability, harmonics, and adjustable speed drives.

Dr. Blaabjerg received 17 IEEE Prize Paper Awards, the IEEE PELS Distinguished Service Award in 2009, the EPE-PEMC Council Award in 2010, the IEEE William E. Newell Power Electronics Award in 2014, and the Villum Kann Rasmussen Research Award in 2014. He was the Editor-in-Chief of the IEEE TRANSACTIONS ON POWER ELECTRONICS from 2006 to 2012. He was nominated to be between the most 250 cited researchers in Engineering in the world in 2014 and 2015 by Thomson Reuters.